Effect of HF and Ethanol Volume Ratio on Porous Silicon Formed by Photoelectrochemical Method on N-type Si(100) Substrates

Suryana, Risa
Department of Physics, Faculty of Mathematics and Natural Sciences, Universitas Sebelas Maret

Nur Azizah Aini
Department of Physics, Faculty of Mathematics and Natural Sciences, Universitas Sebelas Maret

Diantorom, Markus
Department of Physics, Faculty of Mathematics and Natural Sciences, Universitas Negeri Malang

https://doi.org/10.5109/7236856

出版情報：Evergreen. 11 (3), pp.2127-2134, 2024-09. 九州大学グリーンテクノロジー研究教育センター
バージョン：

Effect of HF and Ethanol Volume Ratio on Porous Silicon Formed by Photoelectrochemical Method on N-type Si(100) Substrates

Risa Suryana[1,*], Nur Azizah Aini[1], Markus Diantoro[2]

[1]Department of Physics, Faculty of Mathematics and Natural Sciences, Universitas Sebelas Maret, Indonesia

[2]Department of Physics, Faculty of Mathematics and Natural Sciences, Universitas Negeri Malang, Indonesia

*Author to whom correspondence should be addressed:

E-mail: rsuryana@staff.uns.ac.id

(Received October 29, 2023: Revised March 16, 2024: Accepted June 21, 2024).

Abstract: The photoelectrochemical method using a green laser has been employed in forming PSi on n-type Si (100) surfaces. The volume ratio of HF and ethanol was varied at 1:1, 1:3, and 3:1 to obtain PSi that coincide as an anti-reflective material while current density and etching time were maintained constant. Based on the SEM images, ethanol is dominant in controlling the pore size and distribution. The quantum confinement effect occurs in PSi so that the optical bandgap energy (Eg) of PSi increases with increasing the porosity and decreasing the thickness of PSi. Also, the absorbance of PSi is high for large pore sizes. Due to PSi at a ratio of 1:3 having high porosity and high absorbance, these samples are better materials as anti-reflection layers in Si solar cells application than at ratios of 3:1 and 1:1. In addition, for all ratios, PSi formed a polycrystalline where Si and SiO_2 structures co-exist.

Keywords: Porous silicon; N-type Si(100); Photoelectrochemical; Reflectance; Absorbance

1. Introduction

Porous silicon (PSi) is a silicon substance that exhibits electroluminescence and photoluminescence at room temperature in the visible light region. Moreover, PSi could be easily integrated with existing silicon technology. PSi could be manufactured by using the simple and low-cost technique. Several devices have applied the PSi, such as fuel cell[1)], the anode in lithium-ion batteries[2,3)], and biosensor[4,5)].

There are several etching methods for the fabrication of PSi, namely dry etching and wet etching. The dry etching such as inductively coupled plasma reactive ion etching is commonly used to produce many porous structures[6,7,8,9,10)]. Nonetheless, the dry etching technique has a disadvantage in that this etching technique can damage the surface of the thin film during the etching process. Therefore, this will degrade the properties of the porous structures and also the device's efficiency or performance. On the other hand, the wet etching technique is preferable in the fabrication of PSi compared to the dry etching techniques because it requires simple and inexpensive equipment. The wet etching technique that is commonly used to fabricate PSi is electrochemical using direct current[11,12,13,14)]. They used ethanol to overcome hydrogen bubbles on the surface during the etching process in hydrofluoric acid (HF) so that uniform pores formation with this technique would be attained.

Lehmann and Gosele[15)] proposed silicon decomposition that starts from hole injection and attacks Si-H and Si-Si bonds by fluoride ions to form pores. In semiconductor physics, charge carriers play a crucial role in determining the electrical behavior of materials. In a p-type semiconductor, holes are the majority charge carriers, while in an n-type semiconductor, electrons are the majority charge carriers. Therefore, light is necessary for photoexcitation in n-type silicon, leading to the creation of electron-hole pairs, which contribute to the semiconductor's electrical behavior. In this study, we use the n-type silicon so that light is needed to form PSi. The distribution and shape of pores can be controlled by light with different energies[16,17)].

The photoelectrochemical (PEC) method uses light during the electrochemical process to modify a silicon surface that interacts with HF solution, which induces corrosion on a partial area until a pattern is formed[18)]. The morphology of PSi structures depends on the parameters like crystal orientation, doping density, concentration density, and light wavelength and intensity[19)]. In the previous research, Harb and Mutlak performed the effect of gamma irradiation on the formation of PSi[20)] with different intensities. The pore size and porosity can be adjusted according to the

radiation intensity. Higher intensity caused bigger pores size and lower porosity. Hussein et al. used a red laser to fabricate PSi from n-type silicon with different etching times[21]. They obtained homogeneous structures and increasing pore size with increased etching time. Suryana and Aini formed PSi on n-type Si (100) using a laser-supported electrochemical method[22]. They used different lasers i.e., 405 nm, 532 nm, and 650 nm. By employing 532 nm, the most uniform and dense PSi was produced. However, the distribution of PSi between the above and below Si surface is different due to cathode and anode electrodes being arranged horizontally in HF and ethanol solution. It is considered that the concentration of HF and ethanol solution below is higher than above, causing the PSi density to be higher than above the Si surface. Therefore, to solve the distribution of the PSi density, we apply a vertical photoelectrochemical method with a Si substrate (anode) placed on the bottom cell.

This study examines the effect of HF and ethanol ratio on the morphology, structural, and optical properties of PSi fabricated by the photoelectrochemical method. Scanning Electron Microscopy (SEM), X-ray Diffraction (XRD), Ultraviolet-Visible (UV-Vis) spectrophotometer, and Attenuated Total Reflectance Fourier transform infrared (ATR-FTIR) spectroscopy were performed to obtain the morphological, structural, reflectance, and absorbance of PSi.

2. Method

The research utilized 3" single-polished n-type Si (100) substrates with a thickness of 400 μm owing ρ = 1-5 Ω.cm (D&X Co., Ltd., Tokyo, Japan). It was cut in 1 x 1 cm^2 dimensions. The schematic of the photoelectrochemical method can be seen in Fig. 1. An aluminum back contact was used in direct contact with silicon. Silicon acted as an anode and platinum as a cathode. The ethanol and HF solution worked as the electrolyte solution. Adjustable DC power supply (Picotest P9610A) as a current source and laser-assisted in making a hole in the silicon surface. The anode, cathode, and laser were arranged vertically perpendicular to the substrate by 10 cm.

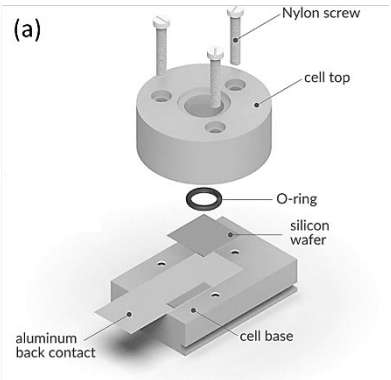

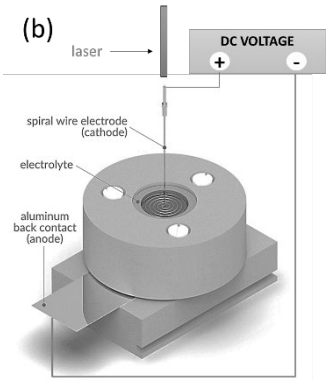

Fig. 1: (a). Parts of electrochemical etch cell and (b). Schematic of the photoelectrochemical method using the etching cell[23]

The photoelectrochemical method started by cleaning substrate with H_2O_2:NH_4OH:H_2O in 1:1:5 v/v for 5 min on a hotplate with a temperature of 100ºC. The sample was cleaned by HF:H_2O in 1:30 v/v for 15 sec. All chemical materials were purchased from Merck Life Science Products (UK). Next, the photoelectrochemical process using the green laser (532 nm, 5 mW) was done during the etching of the substrate in HF (40%): Ethanol (96%) solution in various volume ratios of 1:1, 1:3, and 3:1 for 10 min. The current density applied was maintained at 4 mA/cm^2. After etching, the substrate was overflowed in aquadest. N_2 gas was then used to dry the substrate. Then, the samples were characterized using SEM (FEI-Quanta 250), UV-Vis spectrophotometer (Analytik Jena Specord Plus), XRD (Bruker D8 Advance) with Cu-K alpha 1 wavelength = 1.5406 Å), and ATR-FTIR spectroscopy (Agilent). The distribution and pore size of the sample can be measured from SEM images. Reflectance curves of the samples were obtained by UV-Vis spectrophotometer can show the reflectance peaks, estimate the sample thickness, and calculate the optical bandgap energy. The orientation crystal and crystallite size of the samples could be analyzed using XRD patterns. In addition, ATR-FTIR was carried out to obtain the absorbance value and chemical bonds of PSi.

3. Results and Discussion

Figure 2 displays SEM pictures of the PSi surface after a laser has illuminated Si in the ratios of 1:3, 3:1, and 1:1 using HF:ethanol. The experiment used a green laser with λ=532 nm and P=5 mW that correlates with an energy of 2.33 eV. When Si absorbs the laser energy, the laser energy is greater than the Si bandgap energy, so the electrons in the valence band are excited to the conduction band, leaving holes in the valence band[24]. During laser-induced, n-type crystalline of Si substrate generates redundant holes on the illuminated surface since the substrate was exposed to laser illumination in HF liquid. The depletion layer generates a flow of electrons from the electrolyte solution to the contact

surface. Since the Si substrate and HF acid solution react, the Si surface is rebuilt throughout this process[25]. Hole capture at the surface of n-type Si initiates the etching process. The surface hole triggers a nucleophilic attack on the Si-H bond by F- ions, establishing a Si-F bond[26]. These holes will aid in forming pores by allowing F- ions to disrupt the Si-H and Si-Si bonds[15]. The reaction in etching can be seen in Eq. (1) and Eq. (2), while Eq. (3) is a net reaction. In this equation, h^+ is a hole. The final reaction produces SiF_6^{2-} indicate the initial pore formation and the hydrogen gas (H_2).

Electrochemical:

$$Si + 2\,F^- + 2h^+ \rightarrow [SiF_2] \quad (1)$$

Chemical:

$$[SiF_2] + 4F^- + 2H^+ \rightarrow SiF_6^{2-} + H_2 \quad (2)$$

Net reaction:

$$Si + 6F^- + 2H^+ + 2h^+ \rightarrow SiF_6^{2-} + H_2 \quad (3)$$

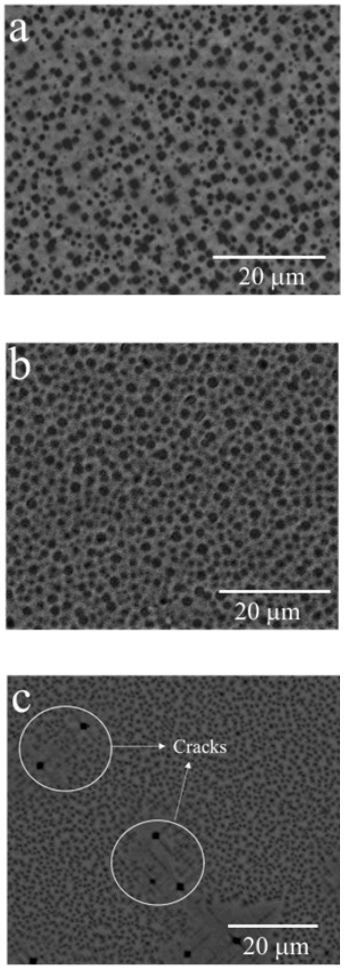

Fig. 2: Morphology of PSi surface after illuminated by green laser during etching process with HF: ethanol ratio a. 1:3, b. 3:1, and c. 1:1. Cracks area (white circles) occurs at a ratio of 1:1.

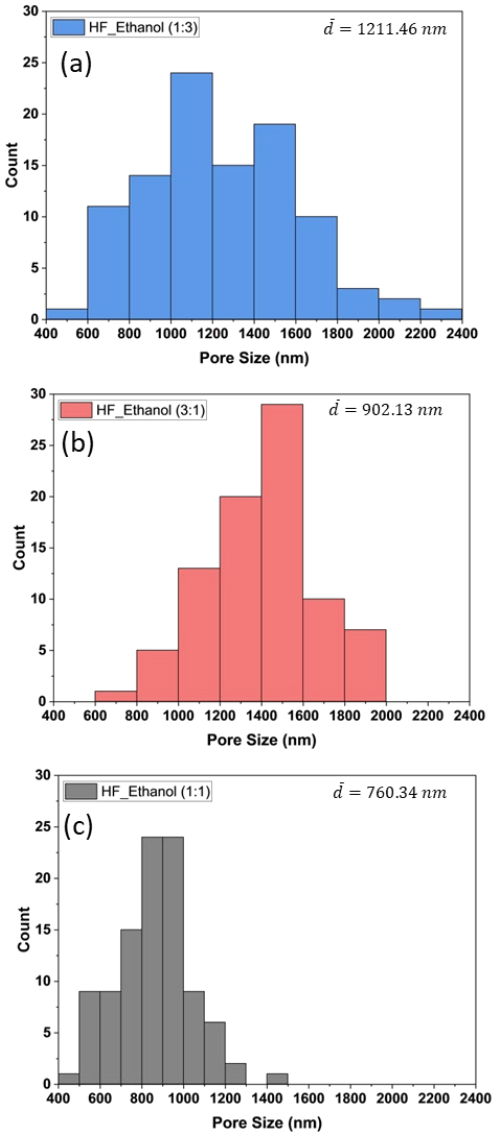

Fig. 3: Distribution of pore size on PSi surface with HF: ethanol ratio in (a). 1:3, (b). 3:1, and (c). 1:1

According to Fig. 2, the black color of the SEM images denotes pores on the Si surface. Figure 3 shows the distribution of pore size for each HF and ethanol ratio obtained using the ImageJ software. As a result, the ratio of 1:3 (sample (a)) has a pore size that is bigger than the other, i.e., 1211.46 nm. Sample (b) and (c) have an average pore size of 902.13 nm and 760.34 nm. The pore density of sample (c) is higher than samples (a) and (b). However, the crack (white circles) occurs in sample (c). Therefore, sample (b), with a ratio of 3:1, has relatively uniform pores.

The reaction product in Eq. (3) is H_2 gas in the form of bubbles on the Si surface that prevents F^- ions from bonding with Si. To reduce the hydrogen bubble during the photoelectrochemical process, alcohol is added as a surfactant such as ethanol[27]. So, when the concentration of ethanol in electrolytes is high, F^- ions can rapidly attack Si-Si bonds to form SiF_6^{2-} or initial formation of

the pore. Therefore, the ratio of HF and ethanol 1:3 has a pore size bigger than ratios 3:1 and 1:1. Furthermore, due to the concentration of ethanol being similar, we assume that the amount of hydrogen bubbles which is reduced on the Si surface is also identical. So, the probability of the F^- ions bond Si is higher in ratio 3:1 than in ratio 1:1. Hence, the pore size of ratio 3:1 is bigger than ratio 1:1. In this study, it is concluded that ethanol plays a key role in controlling the pore size.

Figure 4 displays the experimental spectrum reflectance of PSi samples with various ratios. Because we cannot control the position of the light irradiation from the UV-Vis spectrophotometer that strikes the smooth or cracked PSi surfaces and also based on SEM images that there are cracks on surfaces as shown in Fig. 2, the reflectance curve on the HF:ethanol (1:1) ratio will not be discussed. The reflectance spectrum is divided into three wavelength ranges, namely 210-270 nm, 270-340 nm, and above 340 nm. In the range of 210-270 nm and above 340 nm, the reflectance of PSi at a ratio of 3:1 is higher than that of a ratio of 1:3, while in the range of 270-340 nm, the reflectance at a ratio of 3:1 is lower than that of a ratio of 1:3. This indicates that PSi at a ratio of 1:3 has better anti-reflective properties than PSi at a ratio of 3:1.

Due to changes in microstructure, an alteration of the interference pattern was seen. The quantity of local extremes during the spectrum reflectance is correlated with the thickness of the PSi layer. Klarik et. al.[28] calculated the layer thickness of PSi by the theoretical model using the Looyenga EMA formula from the spectral reflectance. They concluded that more local extreme numbers have greater thickness. Thus, in this study, as shown in Fig. 4, 3:1 has two local extremes while ratio 1:3 has one local extreme means the PSi layer at 3:1 ratio is thicker than at 1:3 ratio.

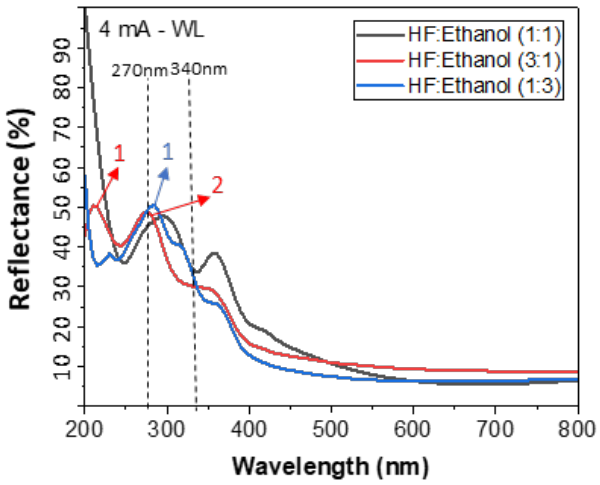

Fig. 4: Reflectance spectra of pore size on PSi surface by HF: ethanol ratio in 1:3, 3:1, and 1:1

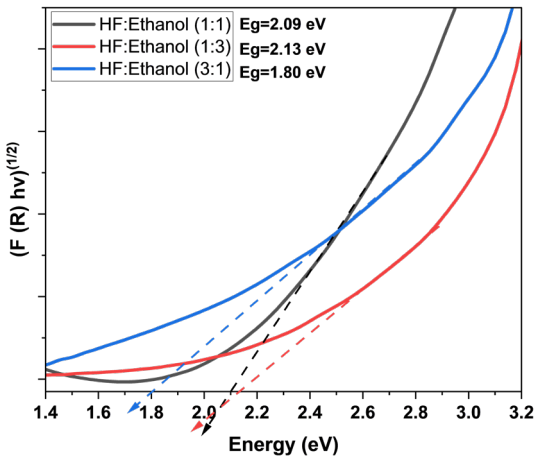

Fig. 5: Optical bandgap energy of PSi for HF:ethanol ratio of 1:3, 3:1, and 1:1

Regarding the reflectance spectra of PSi for each HF:ethanol ratio, as shown in Fig. 4, the optical bandgap energy (Eg) of PSi can be determined using the Kubelka-Munk function in conjunction with the Tauc plot. The Eg values can be obtained from extrapolation of the linear least squares fit of $[F(R_\infty)h\nu]^{1/n}$ to zero, by plotting $[F(R_\infty)h\nu]^{1/n}$ vs $h\nu$[29]. Figure 5 shows the Eg values of PSi samples i.e., 2.13 eV, 1.80 eV, and 2.09 eV for HF:ethanol ratios of 1:3, 3:1, and 1:1, respectively.

The quantum confinement effect in PSi is a fascinating phenomenon that arises due to the nanoscale confinement of charge carriers within porous structures. Gelloz et al.[30] studied the relationship between optical absorption and quantum confinement in PSi nanostructures and investigated chemical dissolution in HF solutions and photoconduction. Based on the absorption spectra, they observed a clear porosity dependence of quantum confinement. If we assume that porosity is defined as the ratio of the amount of pore to the area, from Fig. 3, the porosity of a 1:3 ratio is higher than that of a 3:1 ratio. Pores in PSi act as the localized electronic state, contributing to their unique optical properties. In this study, the Eg increases with increasing porosity, which is 1.80 eV at a ratio of 3:1 to 2.13 eV at a ratio of 1:3, which indicates that more electrons are localized. The decrease of the itinerant electrons causes the increase of bandgap. This result is in good agreement with the reports of Behzad et al.[31,32]. In addition, in this study, the Eg decreases as the thickness of PSi increases. Goh et al.[33] reported that in a two-dimensional system, elementary excitations will experience quantum confinement resulting in finite motion in the thickness direction. They explained the bandgap expansion with a reduction of film thickness.

The XRD patterns of PSi for each ratio have similar orientations, i.e. (110), (200), (320), and (400), and minor peaks owing to the SiO_2 at about 10-20° (Fig.6). Those peaks are determined using commercial Match! Software correlating with #96-901-1057 for Si and #96-

901-1495 for SiO_2. The SiO_2 peaks in this study are in good agreement with Nandanwar et al.,[34] Sankar et al.,[35] and Hijri et al.[36] who found that SiO_2 peak appears at 2 theta of 21-22°.

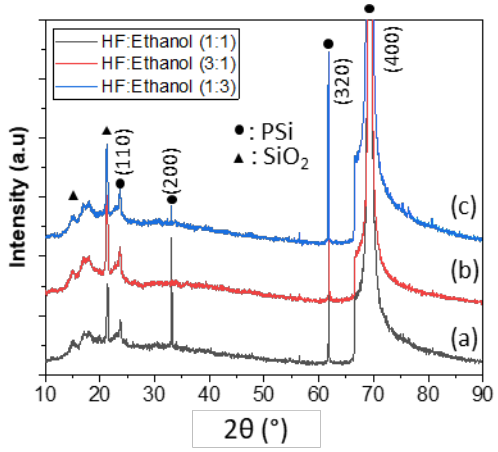

Fig. 6: XRD patterns of PSi with different ratio of HF: ethanol (a). 1:1, (b). 3:1, and (c). 1:3

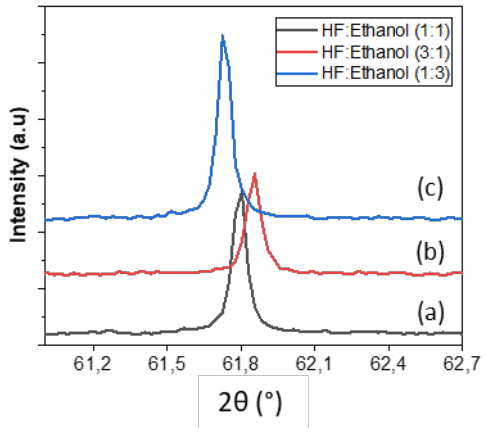

Fig. 7: XRD patterns of PSi at 2 theta about 61° with different ratio of HF: ethanol (a). 1:1, (b). 3:1, and (c). 1:3

To confirm that modification of microstructure occurs in PSi, we show the peaks shifted at about 61°, as shown in Fig. 7, based on the Debye-Scherer equation below[37,38,39]

$$D = K\lambda/\beta cos\theta \qquad (4)$$

where D is the crystallite size, K is a constant (0.9), λ is 0.15418 nm, β is the full width at half maxima (FWHM), and θ is the Bragg's angle. Table 1 shows summary data to obtain the crystallite size for each ratio of HF and ethanol. Differences in crystallite size cause the crystal strain, indicating a microstructure change.

Table 1. Summary of calculation of crystallite size for ratios of 1:1, 3:1, and 1:3

Ratio	β	2θ (°)	θ(rad)	cosθ	β(rad)	D(Å)
1:1	0.069	61.80	1.08	0.47	0.0012	2541.9
3:1	0.075	61.86	1.08	0.47	0.0013	2336.6
1:3	0.068	61.72	1.07	0.47	0.0012	2574.1

The absorbance values of PSi are measured at wavenumber 600-2400 cm^{-1} for different HF and ethanol ratios, as shown in Fig. 8. The absorption of PSi is highest when the HF and ethanol volume ratio is 1:3 compared to the ratio of 3:1 and 1:1. The relation between absorbance value and pores size is proportional. Therefore, the increase in pore size will be proportional to the increase in absorbance value[40].

Figure 8 displays the FTIR spectrum of absorption band intensity on PSi in the wavenumber range of 600-2400 cm^{-1} for each HF:ethanol ratio, i.e., 1:3, 3:1, and 1:1. The absorbance of PSi at a ratio of 1:3 is highest compared to the ratio of 3:1 and 1:1. Therefore, PSi at ratio of 1:3 is better material as anti-reflective layer in solar cell application than PSi at ratio of 3:1 and 1:1. The absorption peaks are dominated by Si-Hn (n=1,2,3), and only one peak owes Si-O-Si. The absorption peak that appears in FTIR measurements indicates the presence of a specific bond in PSi[41]. During the electrochemical process, the illuminated silicon substrate creates electron-hole pairs[42]. The minority carriers reached the electrochemical interface. At the end of the pores, where the electric field is greatest, they can pass through the depletion area to be consumed by the electrochemical reaction. A bond exchange occurs between molecules in solution and Si atoms on the surface during chemical etching, and the amount of photons absorbed in silicon is proportional to hole formation[43]. The hole also penetrates the contact between silicon and electrolytes[44].

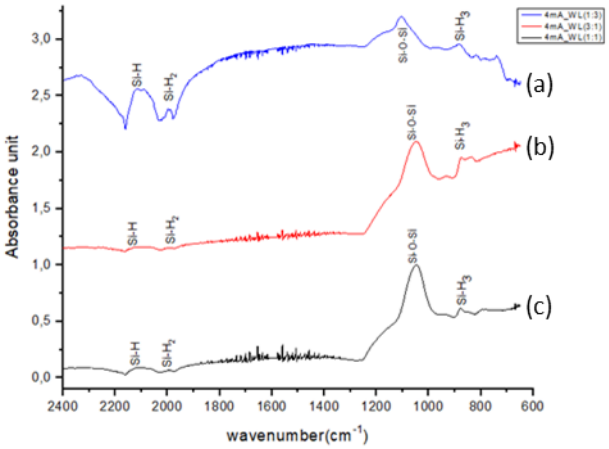

Fig. 8: The absorbance of PSi at HF:ethanol ratio in (a). 1:3, (b). 3:1, and (c). 1:1

Table 2 presents the chemical bond on the absorption spectrum of PSi. The Si-O-Si bond exhibits a peak around 1000 cm^{-1}. The Si-O-Si peak is in good agreement with Dwirekso et al. works[45]. The PSi surface is covered with $Si-H_n$ groups (n= 1,2,3); they appear around 2100, 1994, and 880 cm^{-1}, which is attributed to the typical stretching modes of the Si-H and $Si-H_2$ bond,

then the typical degenerated deformation mode of the Si-H_3. Hydrogen atoms dominate surface of Si during chemical etching due to their characteristic properties of electronegativity to Si than fluorine and its surface, which is not susceptible to nucleophilic attack[46]. At the end of etching, the silicon sample has the main porous structure on surface groups containing Si-H, Si-H_2, Si-H_3, and small amounts of O and F[47].

Table 2. Summary of the wavenumber, bonds, and vibration mode of PSi for each HF: ethanol ratio

HF: Ethanol Ratio	Wavenumber (cm^{-1})	Bonds	Vibration mode
1:3	2125	Si-H	Stretch
	1994	Si-H_2	Stretch
	1102	Si-O-Si	Stretch
	883	Si-H_3	Deformation
3:1	2122	Si-H	Stretch
	1994	Si-H_2	Stretch
	1048	Si-O-Si	Stretch
	876	Si-H_3	Deformation
1:1	2122	Si-H	Stretch
	1994	Si-H_2	Stretch
	1045	Si-O-Si	Stretch
	876	Si-H_3	Deformation

4. Conclusion

The morphological, structural, and optical features of PSi have been studied by successfully fabricating PSi on n-type Si (100) substrates using the photoelectrochemical technique. The pore size of PSi is biggest at an HF: ethanol ratio of 1:3 compared to ratios of 1:1 and 3:1. It is considered that the ethanol concentration has a role in controlling the pore formation to reduce hydrogen bubbles on silicon surfaces. In addition, PSi at a ratio of 1:3 has the highest absorbance value and the highest porosity compared to a ratio of 3:1 and 1:1, so it is better to apply as an anti-reflective layer in Si solar cells.

Acknowledgments

The authors would like to thank Kementerian Pendidikan, Kebudayaan, Riset, dan Teknologi No. 1035.1/UN27.22/PT.01.03/2022 for financial support through the Penelitian Dasar Unggulan Perguruan Tinggi (PDUPT).

References

1) T. D. Dzhafarov, A. H. Bayramov, M. S. Sadigov, S. X. Ragimov, E. A. Bagiyev, S. G. Asadullayeva, J. N. Jalilli, and I. R. Amiraslanov, "Ag/porous silicon-based ammonia-fed fuel cells,"*Aspects in Mining & Mineral Science*, 10(3) 1152-1155 (2022). doi: 10.31031/AMMS.2022.10.000736.
2) N. Badi, A. M. Theodore, A. Roy, S. A. Alghamdi, A. O. M. Alzahrani, and A. Ignatiev,"Preparation and characterization of 3D porous silicon anode material for lithium-ion battery application,"*International Journal of Electrochemical Science*, 17 22064 (2022). doi: 10.20964/2022.06.29.
3) M. Chen, P. Duan, Y. Zhong, Z. Wu, Z. Zhang, Y. Wang, X. Guo, and X. Wang,"Constructing a sheet-stacked Si/C composite by recycling photovoltaic Si waste for Li-ion batteries,"*Industrial & Engineering Chemistry Research*, 61(7) 2809-2816 (2022). DOI: 10.1021/acs.iecr.1c04564.
4) K. Guo, M. Alba, G. P. Chin, Z. Tong, B. Guan, M. J. Sailor, N. H. Voelcker, and B. Prieto-Simon,"Designing electrochemical biosensing platforms using layered carbon-stabilized porous silicon nanostructures,"*Applied Materials & Interfaces*, 14 15565-15575 (2022). https://doi.org/10.1021/acsami.2c02113.
5) R. Vercauteren, A. Leprince, J. Mahillon, and L. A. Francis,"Porous silicon biosensor for the detection of bacteria through their lysate,"*Biosensor* 11 27 (2021). https://doi.org/doi:10.3390/bios11020027.
6) T. Sugaya, D. H. Yoon, H. Yamazaki, K. Nakanishi, T. Sekiguchi, and S. Shoji,"Simple and rapid fabrication process of porous silicon surface using inductively coupled plasma reactive ion etching,"*Journal of Microelectrochemicanical System*, 29(1) 62-67 (2020). DOI: 10.1109/JMEMS.2019.2952209.
7) N. D. Pratiwi, M. Handayani, R. Suryana, and O. Nakatsuka,"Fabrication of porous silicon using photolithography and reactive ion etching (REI),"*Materials Today:Proceedings*, 13 92-96 (2019).
8) M. J. Goodwin, C. A. M. Harteveld, M. J de Boer, and W. L. Vos,"Deep reactive ion etching of cylindrical nanopores in silicon for photonic crystals,"*Nanotechnology*, 34 225301 (2023). https://doi.org/10.1088/1361-6528/acc034.
9) R. Suryana, N. D. Pratiwi, M. Handayani, M. Santika, and O. Nakatsuka,"Patterned porous silicon prepared by reactive ion etching technique,"*IOP Conf. Series: Materials Science and Engineering*, 578 012019 (2019). doi:10.1088/1757-899X/578/1/012019.
10) R. Suryana, M. M. Mas'ud, and O. Nakatsuka,"Influence of reactive ion etching time on fabrication of porous silicon on Si(110) substrates,"*IOP Conf. Series: Materials Science and Engineering*, 109 012139 (2021). doi:10.1088/1757-899X/1096/1/012139.
11) Sehati, S. Wijayanti, and R. Suryana,"Variation of etching time on formation of porous silicon on p-type Si(111) using electrochemical anodization method,"*Journal of Physics: Conference Series*, 1825 012067 (2021).DOI 10.1088/1742-6596/1825/1/012067.
12) S. Wijayanti, Sehati, and R. Suryana,"The formation of porous silicon (PSi) on p-type Si(100) substrate

via the electrochemical anodization method with varying current density,"*Journal of Physics: Conference Series*, 1825 012068 (2021).DOI 10.1088/1742-6596/1825/1/012068.

13) R. Suryana, D. K. Sandi, and O. Nakatsuka,"The morphological study of porous silicon formed by electrochemical anodization method,"*IOP Conf. Series: Materials Science and Engineering*, 333 012034 (2018). DOI 10.1088/1757-899X/333/1/012034.
14) M. T. Tsai, Y. C. Lee, Y. M. Lin, V. K. S. Hsio, and C. C. Chu,"Exploring the influence of solvents on electrochemically etched porous silicon based on photoluminescence and surface morphology analysis,"*Materials*, 17 989 (2024). https://doi.org/10.3390/ma17050989.
15) V. Lehman, and U. Gosele, "Porous silicon formation: A quantum wire effect," *Applied Physics Letters*, 58 856-858 (1991). doi:10.1063/1.104512
16) O. Volovlikova, S. Gavrilov, and P. Lazarenko,"Influence of illumination on porous silicon formed by photo-assisted etching of p-type Si with a different doping level,"*Micromachines*, 11 19 (2020). doi:10.3390/mi11020199.
17) S. N. Sohimee, Z. Hassan, N. M. Ahmed, L. W. Foong, and Q. H. Jin,"Effect of different UV light intensity on porous silicon fabricated by using alternating current photo-assisted electrochemical etching (ACPEC) technique,"*IOP Conf. Series: Journal of Physics: Conf. Series*, 1083 012034 (2018). doi :10.1088/1742-6596/1083/1/012034.
18) P. A. Kohl, "Photoelectrochemical etching of semiconductors," *Journal of Research and Development*, **42**(*5*) 629-638 (1998). doi:10.1147/rd.425.0629.
19) M. N. Ruberto, X. Zhang, R. Scarmozzino, A. E. Willner, D. V. Podlesnik, and R. M Osgood, "The Laser-controlled micrometer-scale Photoelectrochemical Etching of III–V semiconductors," *Journal of The Electrochemical Society*, **138**(*4*) 1174 (1991). doi:10.1149/1.2085737
20) N. Harb, F. Mutlak, "Production and characterization of porous silicon via laser-assisted etching: Effect of gamma irradiation," *International Journal for Light and Electron Optics*, **246**(1) 1-7 (2021). doi:10.1016/j.ijleo.2021.167800
21) D. J. Hussein, H. Muneer, A. Jaduaa, and N. A Ahmed, "Fabrication and characterization of porous silicon," *World Scientific News*, **94**(*2*) 321-328 (2018).
22) R. Suryana, and N. Q. Aini, "Analysis of porous silicon formation on n-type Si (100) using laser-assisted electrochemical anodization method," *Journal of Physics and Its Applications*, **4**(*2*) 1-5 (2022). doi:10.14710/jpa.v4i2.12664.
23) The standard etch cell n.d. https://redox.me/products/the-standard-etch-cell (accessed August 17, 2022).
24) J. Jakubowicz, "Nanoporous silicon fabricated at different illumination and electrochemical conditions," *Superlattice and Microstructures*, **41**(*4*) 205-215 (2007). doi:10.1016/j.spmi.2006.12.003.
25) R. Juhasz, and J. Linnors, "Silicon nanofabrication by electron beam lithography and laser-assisted electrochemical size-reduction," *Microelectronic Engineering*, **61** 563-568 (2002). doi:10.1016/S0167-9317(02)00532-4.
26) R. L. Smith, and S. D Collins, "Porous silicon formation mechanisms," *Journal of Applied Physics*, **71**(8) 1-22 (1992). doi:10.1063/1.350839
27) J. Salonen and V.P. Lehto, "Fabrication and chemical surface modification of mesoporous silicon for biomedical applications," *Chemical Engineering Journal*, **137** 162–172 (2008). doi:10.1016/j.cej.2007.09.001.
28) M. Klarik, M. Hola, and S. Jurecka, "Optical properties of porous silicon solar cells for use in transport," *Communications*, **3**(*21*) 53-58 (2019). doi: 10.26552/com.C.2019.3.53-58.
29) G. D. Gesesse, A. G. Berenguer, M. F. Barthe, and C. O. Ania,"On the analysis of diffuse reflectance measurements to estimate the optical properties of amorphous porous carbons and semiconductors/carbon catalysts,"*Journal of Photochemistry & Photobiology A: Chemistry*, 398 112622 (2020).https://doi.org/10.1016/j.jphotochem.2020.112622.
30) B. Gelloz, K. Ichimura, H. Fuwa, E. Kondoh, and L. Jin,"Optical absorption and quantum confinement in porous silicon nanostructures studied by chemical dissolution in HF solutions and photoconduction," *ECS Journal of Solid State Science and Technology*, 6(1) R1-R2 (2017). DOI: 10.1149/2.0321612jss.
31) K. Behzad, W. M. M. Yunus, Z. A. Talib, A. Zakaria, A. Bahrami, and E. Shahriari,"Effect of etching time on optical and thermal properties of p-type porous silicon prepared by electrical anodisation method,"*Advances in Optical Technologies*, 2012 581743 (2012). doi:10.1155/2012/581743
32) K. Behzad, W. M. M. Yunus, Z. A. Talib, A. Zakaria, A. Bahrami,"Effect of preparation parameters on physical, thermal and optical properties of n-type porous silicon,"*International Journal of Electrochemical Science*, 7 8266-8275 (2012).
33) E. S. M. Goh, T. P. Chen, C. Q. Sun, and Y. C. Liu,"Thickness effect on the band gap and optical properties of germanium thin films,"*Journal of Applied Physics*, 107 024305 (2010).doi:10.1063/1.3291103.
34) R. Nandanwar, P. Singh, and F. Z. Haque, "Synthesis and characterization of SiO_2 nanoparticles by sol-gel process and its degradation of methylene blue, "*American Chemical Science Journal*, **5**(*1*) 1-10

(2015). doi:10.9734/ACSJ/2015/10875.
35) S. Sankar, S. K. Sharma, N. Kaur, B. Lee, D.Y. Kim, S. Lee, and H. Jung," Biogenerated silica nanoparticles synthesized from sticky, red, and brown rice husk ashes by a chemical method, "*Ceramics International*, **42**(*4*) 4875-4885 (2016). doi:10.1016/j.ceramint.2015.11.172.
36) H. A. Hijri, J. F. Fatriansyah, N. Sofyan, and D. Dhaneswara, "Potential use of corn cob waste as the base material of silica thin films for anti-reflective coatings,"*Evergreen*, **9**(1) 102-108 (2022). doi: 10.5109/4774221.
37) A. Fauzi, L. H. Lalasari, N. Sofyan, A. Ferdiansyah, D. Dhaneswara, and A. H. Yuwono, "Titanium dioxide nanosheets derived from Indonesia ilmenite mineral through post-hydrothermal process," *Evergreen*, **9**(2) 470-475 (2022). doi: 10.5109/4794174.
38) Y. Iriani, R. Afriani, D. K. Sandi, and F. Nurosyid, "Co-precipitation synthesis and photocatalytic activity of Mn-doped $SrTiO_3$ for the degradation of methylene blue wastewater," *Evergreen*, **9**(4) 1039-1045 (2022). doi: 10.5109/6625717.
39) M. Naimah, F. D. N. Pratama, and M. Ibadurrohman, "Photocatalytic hydrogen production using Fe-graphene/TiO_2 photocatalysts in the presence of polyalcohols as sacrificial agents," *Evergreen*, **9**(4) 1244-1251 (2022). doi: 10.5109/6625736.
40) M. Handayani, N. D. Pratiwi, and R. Suryana, "Optical absorbance of porous silicon on n-type Si (111) surfaces fabricated by electrochemical anodization method," *Materials Today: Proceedings*, **13**(*1*) 87-91 (2019). doi:10.1016/j.matpr.2019.03.193.
41) M. R. Beghoul, N. Boutaoui, H. Bouridah, R. Remmouche, M. H. Arada, H. Haoues, "Experimental study of n-type porous silicon obtained under illumination," *International Journal for Light and Electron Optics*, **161** 161-165. doi:10.1016/j.ijleo.2018.01.118.
42) M. A. Alwan, A. A. Abas, and A. B. Dheyab, "Study the characteristic of planer and sandwich PSi gas sensor (comparative study)," S*ilicon*, **10** 2527-2534 (2018). doi:10.1007/s12633-018-9787-2.
43) V. Lehmann and H. Foll, "Formation mechanism and properties of electrochemically etched trenches in n-type silicon," *Journal of the Electrochemical Society*, **137** (*2*) 653-659 (1990). doi:10.1149/1.2086525.
44) L. Koker and K. Kolasinski, "Photoelectrochemical etching of Si and porous Si in aqueous HF," *Physical Chemistry Chemical Physics*, **2** (*2*) 277-281 (2000). doi:10.1039/a908383i.
45) I. H. Dwirekso, M. Ibadurrohman, and Slamet, "Synthesis of TiO_2-SiO_2-CuO nanocomposite material and its activities for self-cleaning, "*Evergreen*, 7(2) 285-291 (2020). doi:10.5109/4055234.
46) T. S. Atta, M. J. Zoory, and A. N. Abd, "Porous silicon fabrication by electrochemical and photoelectrochemical methods," *Journal of Physics: Conference Series*, **1963** 012153 (2015). doi:10.1088/1742-6596/1963/1/012153.
47) T. Heng-Chun, C. Chao-Ching, and L. T. Benjamin, "Forming a photoluminescent layer on another surface in the dark through lasering of n-type silicon in an electrolyte," *ACS Omega*, **5** (*41*) 26497–26503 (2020). doi:10.1021/acsomega.0c03165.